

Implementation and validation of two-phase boiling flow models in OpenFOAM

Kai Fu^a, Henryk Anglart^{a,*}

^a*Division of Nuclear Reactor Technology, Royal Institute of Technology, S-106 91 Stockholm, Sweden*

Abstract

Prediction of two-phase boiling flows using the computational fluid dynamics (CFD) approach is very challenging since several sub-models for interfacial mass, momentum and energy transfer in such flows are still not well established and require further development and validation. Once validating a particular model, it is important that all key parameter involved in the model are carefully verified. Such verification is typically performed by separate effect tests, where one parameter at a time is compared to a measured or otherwise known value. Needless to say that for complex models, which are typical for CFD applications to two-phase flow, the number of independent parameters that need to be verified can be quite high. This particular feature makes the validation process of complex CFD models in open source codes very attractive, since full access to the implementation details is possible.

This paper is concerned with implementation and validation of two-phase boiling bubbly flow models using the OpenFOAM, open source environment. The model employs the two-fluid formulation of the conservation equations with the Reynolds-averaged treatment of the turbulent terms. The model consists of six conservation equations for the liquid and the vapor phase, allowing for the thermodynamic non-equilibrium and compressibility of both phases. In addition, the model includes two transport equations for the turbulence kinetic energy and energy dissipation and one transport equation for the interfacial area concentration. New models for wall heat partitioning as well as for the phase change terms in nucleate boiling have been implemented. Sensitivity studies as well as validation of the model against measured data available in the open literature have been performed and it has been shown that a reasonable agreement between predictions and experiments has been achieved.

Keywords: Subcooled; Interfacial area concentration; Bubbly flow; Wall boiling; OpenFOAM;

Abbreviations: DNB, departure from nucleate boiling.

*Corresponding author. Tel.: +46-8-5537-8887

Email addresses: kaifu@kth.se (Kai Fu), henryk@kth.se (Henryk Anglart)

1. Introduction

One of the important issues of the current and future sustainable energy systems is the efficiency and stability of heat removal due to natural or mixed convection, forced convection or boiling heat transfer. In some energy systems natural heat convection is envisaged during normal operation. This type of heat removal is very reliable since it doesn't depend on availability of external pumping resources, and coolant flow through the system is assured by the gravity force. The drawback of the natural circulation is its inherent instability and also relatively low heat transfer efficiency. Thus, in many high heat flux technologies, such as e.g. nuclear reactors, the boiling heat transfer is preferred as the most efficient heat transfer mode. The design of high heat flux systems requires a thorough fluid flow and heat transfer analysis in complex geometries. Traditionally experimental methods have been used for these purposes in the past. The drawback of such methods is their large cost and time consumption, inherently related to all required experimental work. In addition, experimental methods are rather difficult to be used for a design optimization, where various geometry and/or operation condition variations are to be tested. For such purposes the most efficient design and optimization approach is based on computational tools, which are able to capture the geometry details and to include the governing phenomena. Currently the computational fluid dynamics (CFD) technology is widely used to design and to optimize heat transfer and fluid flow systems if single-phase flow conditions prevail. For two-phase flow applications, and in particular for boiling heat transfer conditions the CFD technology is still not mature enough. In particular, there is still lack of thoroughly validated and generally valid closure laws for subcooled and saturated nucleate flow boiling heat transfer, with a potential to be extended to predict the departure from nucleate boiling (DNB). The major aim of this paper is to contribute with new model development and validation in this particular area using open source CFD code OpenFOAM. The first model suitable for CFD applications was developed by [Kurul and Podowski \(1990\)](#), who proposed a heat flux partitioning scheme to separately deal with vapor generation, sensible heat and quenching terms in the proximity of the heated wall. In the bulk bubbly flow, [Hibiki and Ishii \(2002\)](#) proposed a two-equation model to predict the bubble size (and thus the interfacial area concentration) as a function of local flow conditions.

2. Field equation in two-phase bubbly flow

The present model includes mass, linear momentum and energy conservation equations for liquid and vapor phase. In addition, transport equations for the interfacial area concentration and for the turbulence are used to close the model. The details of the employed governing equations are given below.

2.1. Phase continuity equation

$$\frac{\partial(\alpha_k \rho_k)}{\partial t} + \nabla \cdot (\alpha_k \rho_k \mathbf{U}_k) = \Gamma_k \quad (1)$$

Γ_k means the mass gained by phase k . ($k = l, v$)

2.2. Linear momentum conservation equation

$$\frac{\partial(\alpha_k \rho_k \mathbf{U}_k)}{\partial t} + \nabla \cdot (\alpha_k \rho_k \mathbf{U}_k \mathbf{U}_k) = -\alpha_k \nabla p + \nabla \cdot [\alpha_k (\boldsymbol{\tau}_k + \boldsymbol{\tau}_k^t)] + \alpha_k \rho_k \mathbf{g} + \Gamma_k \mathbf{U}_{ki} + \mathbf{M}_{ki} \quad (2)$$

Here the interfacial velocity is modeled as

$$\mathbf{U}_{ki} = \begin{cases} \mathbf{U}_l & \text{if } \Gamma_v > 0, \text{ evaporation} \\ \mathbf{U}_v & \text{if } \Gamma_v < 0, \text{ condensation} \end{cases} \quad (3)$$

using the upwind scheme.

According to the Boussinesq hypothesis, the turbulent stress strain relation is analogous to that of Newtonian fluids and consequently the effective stress appears as a function of fluid properties and velocity, which is used by Rusche (2002) in OpenFOAM,

$$\boldsymbol{\tau}_k^{\text{eff}} = \boldsymbol{\tau}_k + \boldsymbol{\tau}_k^t = \rho_k \nu_k^{\text{eff}} \left(\nabla \mathbf{U}_k + (\nabla \mathbf{U}_k)^T - \frac{2}{3} \mathbf{I} \nabla \cdot \mathbf{U}_k \right) - \frac{2}{3} \mathbf{I} \rho_k k_k \quad (4)$$

and,

$$\nu_k^{\text{eff}} = \nu_k + \nu_k^t \quad (5)$$

2.3. Enthalpy equation

$$\frac{\partial(\alpha_k \rho_k h_k)}{\partial t} + \nabla \cdot (\alpha_k \rho_k h_k \mathbf{U}_k) = -\nabla \cdot [\alpha_k (\mathbf{q}_k'' + \mathbf{q}_k^t)] + \Gamma_k h_{ki} + a_i q_{ki}'' + a_w q_{kw}'' \quad (6)$$

where a_w refers to heated area per unit controlled volume of fluid between the wall and the liquid phase.

Kurul and Podowski (1991) discussed the mass conservation and energy conservation at the interface and first proposed the corresponding equations in two-phase flow. Here we formulate the mass flux Γ_l from phase v to phase l furthermore as,

$$\Gamma_l = \begin{cases} \frac{a_i q_{li}'' + a_i q_{vi}''}{h_v - h_{l,\text{sat}}} & \text{condensation} \\ \frac{a_i q_{li}'' + a_i q_{vi}''}{h_{v,\text{sat}} - h_l} & \text{evaporation} \end{cases} \quad (7)$$

where the interfacial enthalpy h_{ki} ($k = l, v$) is modeled with the upwind approximation. The modeling of interfacial heat transfer $a_i q_{li}''$ and $a_i q_{vi}''$ will be introduced in the following section.

Equation 7 could be applied to the heat transfer in the bulk. For those cells which are adjacent to the wall directly, we have totally different heat transfer mechanism since there are interaction among the liquid, vapor and walls. Here we assume that only evaporation is allowed in those cells, which is consistent with the situation in boiling flows. In those cells, the total heat transfer per unit volume to phase l is given as,

$$q_l''' = a_i q_{li}'' - \Gamma_{vl} h_l + a_w q_{lw}'' \quad (8)$$

and the total heat transfer to phase v as,

$$q_v''' = a_i q_{vi}'' + \Gamma_{vl} h_v + a_w q_{vw}'' \quad (9)$$

The energy balance in those cells could be written as

$$q_i''' + q_v''' = a_w q_w'' \quad (10)$$

Usually we make an assumption that in subcooled flow boiling, the temperature of the vapor phase is constant and equal to the saturation temperature. In addition, we neglect a direct heating of vapor from the wall, that is: $a_w q_{vw}'' = 0$. With these assumptions it is straightforward to calculate the heat flux to each phase in cells adjacent to the heated walls.

Using the Fourier's law of conduction for the liquid phase, the molecular heat flux in Eqn. 6 can be written as,

$$\mathbf{q}_k'' = -\frac{\lambda_l}{c_{pl}} \nabla h_l \quad (11)$$

where λ and c_p are respectively the thermal conductivity and the specific heat.

The turbulent heat flux is found as follows,

$$\mathbf{q}_i^t = -\frac{\lambda_l^t}{c_{pl}} \nabla h_l \quad (12)$$

where the turbulent thermal conductivity is given as,,

$$\lambda_l^t = \frac{c_{pl} \rho_l \nu_l^t}{\text{Pr}_l^t} \quad (13)$$

where Pr_l^t is the turbulent Prandtl number of phase l . A constant value of 0.9 has been chosen for Pr_l^t in the calculations presented in this paper.

In OpenFOAM, equation 6 of liquid phase is reorganized into a phase intensive form,

$$\frac{\partial h_l}{\partial t} + \mathbf{U}_l \cdot \nabla h_l - \nabla \cdot (\kappa_l^{\text{eff}} \nabla h_l) - \kappa_l^{\text{eff}} \frac{\nabla(\beta \rho_l)}{\beta \rho_l} \cdot \nabla h_l = \begin{cases} \frac{\Gamma_{lv} h_{l,\text{sat}} - \Gamma_{lv} h_l + a_i q_{li}''}{\beta \rho_l} & \text{bulk condensation} \\ \frac{a_i q_{li}''}{\beta \rho_l} & \text{bulk evaporation} \\ \frac{a_i q_{li}'' + a_w q_{lw}''}{\beta \rho_l} & \text{near wall cells} \end{cases} \quad (14)$$

where,

$$\kappa_l^{\text{eff}} = \frac{\lambda_l}{\rho_l c_{pl}} + \frac{\nu_l^t}{\text{Pr}_l^t} \quad (15)$$

The term $\frac{a_w q_{lw}''}{\beta \rho_l}$ on the right hand side (RHS) of Eqn. 14 results from the thermal boundary condition at heated walls. Thus we treat this term by a gradient boundary condition in the energy transport equation.

In a similar manner, equation 6 of the vapor phase is given as follows,

$$\frac{\partial h_v}{\partial t} + \mathbf{U}_v \cdot \nabla h_v - \nabla \cdot (\kappa_v^{\text{eff}} \nabla h_v) - \kappa_v^{\text{eff}} \frac{\nabla(\alpha \rho_v)}{\alpha \rho_v} \cdot \nabla h_v = \begin{cases} \frac{a_i q''_{vi}}{\alpha \rho_v} & \text{bulk condensation} \\ \frac{\Gamma_{vl} h_{v,\text{sat}} - \Gamma_{vl} h_v + a_i q''_{vi}}{\alpha \rho_v} & \text{bulk evaporation} \\ \frac{a_i q''_{vi}}{\alpha \rho_v} & \text{near wall cells} \end{cases} \quad (16)$$

where,

$$\kappa_v^{\text{eff}} = \frac{\lambda_v}{\rho_v c_{pv}} + \frac{\nu_v^t}{\text{Pr}_v^t} \quad (17)$$

2.4. Interfacial area concentration transport equation

The interfacial area concentration corresponds to the area of the gas bubbles per unit volume. For spherical bubbles,

$$a_i = \frac{6\alpha}{D_S} \quad (18)$$

where D_S is the bubble Sauter diameter, equal to the diameter of a sphere of an equivalent volume.

Hibiki and Ishii (2002) modeled sink and source terms of the interfacial area concentration based on mechanisms of bubble-bubble and bubble-turbulent eddy random collisions, and they also introduced the effect by gas expansion,

$$\frac{\partial a_i}{\partial t} + \nabla \cdot (a_i \mathbf{U}_v) = \frac{2}{3} \frac{a_i}{\alpha} \left(\frac{\partial \alpha}{\partial t} + \nabla \cdot (\alpha \mathbf{U}_v) \right) + \Phi_{\text{BB}} + \Phi_{\text{BC}} + \Phi_{\text{NUC}} \quad (19)$$

The first term on the RHS of Eqn. 19 refers to the contribution of phase change and expansion due to the pressure change. Φ_{BB} and Φ_{BC} represent the bubble number variations induced by the breakup and coalescence phenomena, respectively. In the Hibiki and Ishii (2002) model, they are defined as,

$$\Phi_{\text{BC}} = -\frac{1}{3\psi} \left(\frac{\alpha}{a_i} \right)^2 \cdot \Gamma_C \frac{\alpha^2 \epsilon_l^{1/3}}{D_S^{11/3} (\alpha_{\text{max}} - \alpha)} \exp \left(-K_C \frac{D_S^{11/3} \rho_l^{1/2} \epsilon_l^{1/3}}{\sigma^{1/2}} \right) \quad (20)$$

with $\Gamma_C = 0.0314$ and $K_C = 1.29$, $\alpha_{\text{max}} = 0.74$, and

$$\Phi_{\text{BB}} = \frac{1}{3\psi} \left(\frac{\alpha}{a_i} \right)^2 \cdot \Gamma_B \frac{\alpha(1-\alpha)\epsilon_l^{1/3}}{D_S^{11/3} (\alpha_{\text{max}} - \alpha)} \exp \left(-K_B \frac{\sigma}{D_S^{5/3} \rho_l \epsilon_l^{2/3}} \right) \quad (21)$$

with $\Gamma_B = 0.0209$ and $K_B = 1.59$. Here $\psi = 1/(36\pi)$ for spherical bubbles.

Φ_{NUC} refers to an increase of interfacial area concentration by a bubble nucleation at the heated wall. Bae et al. (2008) proposed the nucleation source term as,

$$\Phi_{\text{NUC}} = \pi d_{l_0}^2 \cdot N'' f a_w \quad (22)$$

where d_{lo} is the bubble lift-off diameter, N'' the active nucleation site density, and f the bubble departure frequency.

Yao and Morel (2004) proposed the breakup and coalescence term as,

$$\Phi_{BC} = -\frac{1}{3\psi} \left(\frac{\alpha}{a_i}\right)^2 \cdot K_{c1} \frac{\alpha^2 \epsilon_l^{1/3}}{D_S^{11/3}} \frac{1}{1 - (\alpha/\alpha_{\max})^{1/3} + K_{c2} \alpha \sqrt{\text{We}/\text{We}_{cr}}} \exp\left(-K_{c3} \sqrt{\frac{\text{We}}{\text{We}_{cr}}}\right) \quad (23)$$

where $K_{c1} = 2.86$, $K_{c2} = 1.922$, $K_{c3} = 1.017$, $\text{We}_{cr} = 1.24$ and $\alpha_{\max} = 0.52$.

$$\Phi_{BB} = \frac{1}{3\psi} \left(\frac{\alpha}{a_i}\right)^2 \cdot K_{b1} \frac{\alpha(1-\alpha)\epsilon_l^{1/3}}{D_S^{11/3}} \frac{1}{1 + K_{b2}(1-\alpha)\sqrt{\text{We}/\text{We}_{cr}}} \exp\left(-\frac{\text{We}_{cr}}{\text{We}}\right) \quad (24)$$

where $K_{b1} = 1.6$, and $K_{b2} = 0.42$.

Lo and Zhang (2009) proposed a S_γ model in which the breakup terms can be written down as,

$$\Phi_{BB} = \pi \int_{D_{Scr}}^{\infty} \frac{(2^{1/3} - 1)D_S^2}{\tau_{br}} n P dD_S \quad (25)$$

Here $n = \frac{6\alpha}{\pi D_S^3}$ is the bubble number density. P represents the log-normal distribution of bubble diameter,

$$P = \frac{1}{\sqrt{2\pi}D_S\hat{\sigma}} \exp\left(-\frac{(\ln D_S - \ln \bar{D}_S)^2}{2\hat{\sigma}^2}\right) \quad (26)$$

where we use $\hat{\sigma} = 0.5$ in the current solver. In the original paper, the breakup source term is modeled in two regimes: the viscous breakup regime and inertia breakup regime. And the overall source term should be summed up over the two regimes. However, since the mechanism is not well explained in the viscous regime, only the inertial breakup part is included in the current solver.

The Kolmogorov length scale L_k is used to evaluate the regime that breakup takes place.

$$L_k = \left(\frac{\nu^3}{\epsilon}\right)^{1/4} \quad (27)$$

Considering that only those bubbles of big size can break, the critical size in the inertia regime becomes as follows,

$$D_{Scr} = (1 + C_\alpha \alpha) \left(\frac{\sigma \text{We}_{cr}}{2\rho_l}\right)^{3/5} \epsilon^{-2/5} \quad (28)$$

$$\tau_{br} = 2\pi k_{br} \sqrt{\frac{(3\rho_v + 2\rho_l)D_S^3}{192\sigma}} \quad (29)$$

with $C_\alpha = 0$ and $k_{br} = 0.2$.

The source term from bubble coalescence is modeled as,

$$\Phi_{BC} = \pi(2^{1/3} - 2) \left(\frac{6\alpha}{\pi}\right)^2 k_{coll} U_r P_{coal} D_S^{-2} \quad (30)$$

where,

$$k_{coll} = \left(\frac{2\pi}{15} \right)^{1/2} \quad (31)$$

$$U_r = (\epsilon D_S)^{1/3} \quad (32)$$

$$P_{coal} = \frac{\Phi_{\max}}{\pi} \left(1 - \frac{k_{cl,2}^2 (\text{We} - \text{We}_0)^2}{16\Phi_{\max}^2} \right)^{1/2} \quad (33)$$

$$\Phi_{\max} = \frac{8h_0^2 \rho_l \sigma}{\text{We}_0 \mu_v^2 D_S} \quad (34)$$

with the following coefficient: $k_{cl,2} = 12.7$, $\text{We}_0 = 0.8\text{We}_{cr}$ and $h_0 = 8.3h_{cr}$

$$h_{cr} = \left(\frac{A_H D_S}{24\pi\sigma} \right)^{1/3} \quad (35)$$

where $A_H = 5.0 \times 10^{-21}$ is the Hamaker constant.

2.5. Turbulence modeling

2.5.1. Turbulence of liquid phase

Rusche (2002) proposed the standard $k - \epsilon$ model as follows,

$$\frac{\partial(\beta\rho_l k_l)}{\partial t} + \nabla \cdot (\beta\rho_l \mathbf{U}_l k_l) = \nabla \cdot \left[\beta \left(\frac{\mu_l^{\text{eff}}}{\sigma_k} \right) \nabla k_l \right] + \beta G - \beta\rho_l \epsilon_l \quad (36)$$

$$\frac{\partial(\beta\rho_l \epsilon_l)}{\partial t} + \nabla \cdot (\beta\rho_l \mathbf{U}_l \epsilon_l) = \nabla \cdot \left[\beta \left(\frac{\mu_l^{\text{eff}}}{\sigma_\epsilon} \right) \nabla \epsilon_l \right] + \frac{\beta\epsilon_l}{k_l} (C_{\epsilon 1} G - C_{\epsilon 2} \rho_l \epsilon_l) \quad (37)$$

Here G stands for the production of turbulent kinetic energy and is defined as,

$$G = 2\mu_l^\dagger (\nabla \mathbf{U}_l \cdot \text{dev}(\nabla \mathbf{U}_l + (\nabla \mathbf{U}_l)^T)) \quad (38)$$

In the above model, no effect of the dispersed phase on the turbulence in the continuous phase is taken into account. This deficiency is removed in the model proposed by Yao and Morel (2004), where an additional source term, representing the above-mentioned effect, is included,

$$\begin{aligned} \frac{\partial(\beta\rho_l k_l)}{\partial t} + \nabla \cdot (\beta\rho_l \mathbf{U}_l k_l) = & \nabla \cdot \left[\beta \left(\frac{\mu_l^\dagger}{\sigma_k} \right) \nabla k_l \right] - \beta\rho_l \epsilon_l + \beta\boldsymbol{\tau}_l : \nabla \mathbf{U}_l \\ & - (\mathbf{M}_v^d + \mathbf{M}_v^{vm}) \cdot (\mathbf{U}_v - \mathbf{U}_l) - \sigma(\Phi_{BC} + \Phi_{BB}) + k_l \Gamma_l \quad (39) \\ \frac{\partial(\beta\rho_l \epsilon_l)}{\partial t} + \nabla \cdot (\beta\rho_l \mathbf{U}_l \epsilon_l) = & \nabla \cdot \left[\beta \left(\frac{\mu_l^\dagger}{\sigma_\epsilon} \right) \nabla \epsilon_l \right] - C_{\epsilon 2} \beta\rho_l \frac{\epsilon_l^2}{k_l} + C_{\epsilon 1} \beta \frac{\epsilon_l}{k_l} \boldsymbol{\tau}_l : \nabla \mathbf{U}_l - \frac{2}{3} \beta\rho_l \epsilon_l \nabla \cdot \mathbf{U}_l \\ & - C_{\epsilon 3} (\mathbf{M}_v^d + \mathbf{M}_v^{vm}) \cdot (\mathbf{U}_v - \mathbf{U}_l) \left(\frac{\epsilon_l}{D_S^2} \right)^{1/3} + \epsilon_l \Gamma_l \quad (40) \end{aligned}$$

The liquid Reynolds stress tensor is modeled as,

$$\boldsymbol{\tau}_l = \rho_l \nu_l^t (\nabla \mathbf{U}_l + (\nabla \mathbf{U}_l)^T) - \frac{2}{3} \rho_l (k_l + \nu_l^t \nabla \cdot \mathbf{U}_l) \mathbf{I} \quad (41)$$

The turbulent viscosity of liquid phase is given by [Sato and Sekoguchi \(1975\)](#) as,

$$\nu_l^t = C_\mu \frac{k^2}{\epsilon} + \frac{1}{2} C_{\mu b} D_S \alpha |\mathbf{U}_v - \mathbf{U}_l| \quad (42)$$

The coefficients used in this work are $\sigma_k = 1.0$, $\sigma_\epsilon = 1.3$, $C_{\epsilon 1} = 1.44$, $C_{\epsilon 2} = 1.92$, $C_{\epsilon 3} = 0.6$, $C_\mu = 0.09$ and $C_{\mu b} = 1.2$.

2.5.2. Turbulence of vapor phase

The turbulence of vapor phase is assumed to be dependent on that of the liquid phase. To this end, a turbulence response coefficient C_t , defined as the ratio of the root mean square values of dispersed phase velocity, is introduced. In this approach, the effective viscosity of the vapor phase is expressed as

$$\nu_v^{\text{eff}} = \nu_v + C_t^2 \nu_l^t \quad (43)$$

In a more elaborated model, C_t could be calculated as a function of local parameters, such as e.g. void fraction. However, in the present approach the influence of the liquid phase is neglected and C_t is set equal to zero.

3. Interfacial momentum transfer closure laws

The interfacial forces acting on a bubble are caused by the liquid which surrounds it. Ignoring the effect of the change of the mean curvature on the mixture momentum source, we have,

$$\mathbf{M}_v + \mathbf{M}_l = 0 \quad (44)$$

The closure relationships for the interfacial forces are expressed in terms of the following non-dimensional numbers,

Eotvos number,

$$\text{Eo} = \frac{(\rho_l - \rho_v) g D_S^2}{\sigma} \quad (45)$$

Reynolds number,

$$\text{Re}_b = \frac{|\mathbf{U}_v - \mathbf{U}_l| D_S}{\nu_l} \quad (46)$$

$$\text{Re}_{bm} = \frac{\rho_l |\mathbf{U}_v - \mathbf{U}_l| D_S}{\mu_m} \quad (47)$$

Here,

$$\mu_m = \mu_l \left(1 - \frac{\alpha}{\alpha_{\max}} \right)^{-2.5 \alpha_{\max} \mu^*} \quad (48)$$

$$\mu^* = \frac{\mu_v + 0.4 \mu_l}{\frac{\mu_v}{8} + \mu_l} \quad (49)$$

The interfacial momentum transfer terms include different kinds of forces, each of them representing a separate physical phenomenon, including the drag force, the lift force, the wall lubrication force, the turbulent dispersion force and the virtual mass force, which constitute the total interfacial force as follows,

$$\mathbf{M}_v = \mathbf{M}_v^d + \mathbf{M}_v^l + \mathbf{M}_v^{wl} + \mathbf{M}_v^{td} + \mathbf{M}_v^{vm} \quad (50)$$

3.1. Drag force

This force represents a resistance of the relative motion between two phases.

$$\mathbf{M}_v^d = -\frac{3}{4} \frac{C_{ds}}{D_S} \rho_l \alpha |\mathbf{U}_v - \mathbf{U}_l| (\mathbf{U}_v - \mathbf{U}_l) \quad (51)$$

The following two models for the drag force coefficient are included in the current solver: [Schiller and Naumann \(1935\)](#),

$$C_{ds} = \max \left(\frac{24}{\text{Re}_b} (1 + 0.15 \text{Re}_b^{0.687}), 0.44 \right) \quad (52)$$

[Ishii and Zuber \(1979\)](#),

$$C_{ds} = \max \left(\frac{24}{\text{Re}_{bm}} (1 + 0.15 \text{Re}_{bm}^{0.687}), 0.44 \right) \quad (53)$$

3.2. Lift force

When a particle travels through the fluid with a non-uniform lateral velocity field, a lateral force will be acting between the fluid and the particle,

$$\mathbf{M}_v^l = C_l \rho_l \alpha (\mathbf{U}_v - \mathbf{U}_l) \times \nabla \times \mathbf{U}_l \quad (54)$$

In the present model the lift coefficient C_l is calculated from the [Tomiyama \(1998\)](#) model,

$$C_l = \begin{cases} \min(0.288 \tanh(0.121 \text{Re}_b), f(\text{Eo}_d)) & \text{Eo}_d < 4 \\ f(\text{Eo}_d) & 4 < \text{Eo}_d < 10 \\ -0.27 & \text{Eo}_d > 10 \end{cases} \quad (55)$$

$$f(\text{Eo}_d) = 0.001509 \text{Eo}_d^3 - 0.0159 \text{Eo}_d^2 - 0.0204 \text{Eo}_d + 0.474 \quad (56)$$

Here,

$$\text{Eo}_d = \frac{(\rho_l - \rho_v) g d_h^2}{\sigma} \quad (57)$$

$$d_h = D_S (1 + 0.163 \text{Eo}^{0.757})^{1/3} \quad (58)$$

It should be noted that the force is turned off in the cells adjacent to walls in order to avoid unexpected fluctuation of void fraction in those cells in numerical simulation.

3.3. Wall lubrication force

This force was first proposed by [Antal et al. \(1991\)](#) in order to explain the near wall void fraction features.

$$\mathbf{M}_v^{wl} = C_w \rho_l \alpha |\mathbf{U}_r - (\mathbf{U}_r \cdot \mathbf{n}_w) \mathbf{n}_w|^2 \mathbf{n}_w \quad (59)$$

The following two models for the wall lubrication force coefficient are included in the current solver:

[Tomiyama \(1998\)](#),

$$C_w = \frac{1}{2} C_{wl} D_S \left(\frac{1}{y_w^2} - \frac{1}{(D_{pipe} - y_w)^2} \right) \quad (60)$$

$$C_{wl} = \begin{cases} 0.47 & \text{Eo} < 1 \\ \exp(-0.933\text{Eo} + 0.179) & 1 < \text{Eo} < 5 \\ 0.00599\text{Eo} - 0.0187 & 5 < \text{Eo} < 33 \\ 0.179 & \text{Eo} > 33 \end{cases} \quad (61)$$

[Frank \(2005\)](#),

$$C_w = C_{wl} \max \left(0, \frac{1}{C_{wd}} \frac{1 - y_w / C_{wc} D_S}{y_w (y_w / C_{wc} D_S)^{p-1}} \right) \quad (62)$$

It is suggested that $C_{wc} = 10.0$, $C_{wd} = 6.8$ and $p = 1.7$.

3.4. Turbulent dispersion force

The turbulent dispersion force accounts for the turbulent fluctuations of the liquid phase and the effects, which the fluctuations have on the distribution of the gas phase. The following models are currently included in the solver:

[Gosman et al. \(1992\)](#),

$$\mathbf{M}_v^{td} = -C_d \frac{3}{4} \frac{\rho_l}{D_S} \frac{v_l^t}{\sigma_\alpha} |\mathbf{U}_r| \nabla \alpha \quad (63)$$

[Lopez de Bertodano \(1992\)](#),

$$\mathbf{M}_v^{td} = -C_{td} \rho_l k_l \nabla \alpha \quad (64)$$

3.5. Virtual mass force

$$\mathbf{M}_v^{vm} = -C_{vm} \rho_l \left(\frac{D\mathbf{U}_v}{Dt} - \frac{D\mathbf{U}_l}{Dt} \right) \quad (65)$$

Currently it is assumed that $C_{vm} = 0.5$.

4. Liquid-vapor interfacial heat transfer closure laws

Yao and Morel (2004) proposed the following model for the liquid phase interfacial heat transfer,

$$a_i q''_{li} = \begin{cases} c_{li} a_i (h_{l,\text{sat}} - h_l) & \text{bulk} \\ \text{not specified} & \text{near wall cells} \end{cases} \quad (66)$$

and,

$$c_{li} = \frac{\lambda_l}{c_{pl} D_S} \text{Nu} \quad (67)$$

The Nusselt number is

$$\text{Nu} = \begin{cases} 2 + 0.6\text{Re}^{0.5}\text{Pr}^{0.33} & \text{if } \text{Ja} < 0, \text{ condensation} \\ \max(\text{Nu}_1, \text{Nu}_2, \text{Nu}_3) & \text{if } \text{Ja} > 0, \text{ evaporation} \end{cases} \quad (68)$$

where,

$$\text{Ja} = \frac{\rho_l c_{pl} (T_l - T_{\text{sat}})}{\rho_v h_{fg}}, \quad \text{Re} = \frac{D_S U_r}{\nu_l}, \quad \text{Pe} = \frac{D_S U_r}{\kappa_l} \quad (69)$$

$$\text{Nu}_1 = \sqrt{\frac{4\text{Pe}}{\pi}}, \quad \text{Nu}_2 = \frac{12}{\pi} \text{Ja}, \quad \text{Nu}_3 = 2 \quad (70)$$

The interface to vapor heat transfer is expressed in the following manner,

$$a_i q''_{vi} = c_{vi} (h_{v,\text{sat}} - h_v) \quad (71)$$

$$c_{vi} = \frac{\alpha \rho_v}{\delta t} \quad (72)$$

where δt is numerical time step. The above equations make sure that the vapor temperature is very close to the saturation temperature.

5. Subcooled nucleate boiling model

The wall heat transfer model for subcooled boiling flow was first proposed by Kurul and Podowski (1990), who partitioned the wall heat flux into three components: single phase convection, transient conduction as well as evaporation. The heat transfer coefficient for each process is correlated against experiment respectively. More recent work is done by Steiner et al. (2005) and they believe that the total heat flux is assumed to be additively composed of a forced convective and a nucleate boiling component.

5.1. Single phase convective heat transfer

The single phase forced convection heat flux outside the influence area is calculated by Kurul and Podowski (1990) as,

$$q''_c = h_{fc} A_{1\Phi} (T_w - T_l) \quad (73)$$

where h_{fc} is the single phase liquid heat transfer coefficient, $A_{1\Phi}$ is the area fraction dominated by single phase convection, T_w is wall temperature and T_l is the subcooled liquid temperature.

The single phase forced convective heat transfer coefficient h_{fc} is modeled as,

$$h_{fc} = \rho_l c_{pl} \frac{u_\tau}{T^+} \quad (74)$$

where the dimensionless temperature is modeled by [Kader \(1981\)](#),

$$T^+ = \text{Pr } y^+ \exp(-\eta) + (2.12 \ln y^+ + \beta_t) \exp(-1/\eta) \quad (75)$$

and,

$$\beta_t = (3.85 \text{Pr}^{1/3} - 1.3)^2 + 2.12 \ln \text{Pr} \quad (76)$$

$$\eta = \frac{0.01(\text{Pr } y^+)^4}{1 + 5\text{Pr}^3 y^+} \quad (77)$$

$$y^+ = \frac{\rho_l u_\tau |\mathbf{U}_l|}{\mu_l} \quad (78)$$

The friction velocity is coupled with $k - \epsilon$ model,

$$u_\tau = C_\mu^{0.25} \sqrt{k}; \quad (79)$$

5.2. Quenching heat transfer

The quenching (or transient conduction) heat flux is modeled as,

$$q_q'' = h_q A_b (T_w - T_l) \quad (80)$$

where A_b represents the bubble influenced area fraction. According to [Kurul and Podowski \(1990\)](#), the bubble influenced area is determined by

$$A_b = \min \left[1, N'' K \left(\frac{\pi d_{lo}^2}{4} \right) \right] \quad (81)$$

Here K determines the size of the bubble influence area around the nucleation site on the surface. $K = 4$ is recommended by [Del Valle and Kenning \(1985\)](#).

The quenching heat transfer coefficient is given by [Del Valle and Kenning \(1985\)](#),

$$h_q = 2 \frac{\lambda_l}{\sqrt{\pi \kappa_l t}} \quad (82)$$

where $t = 0.8/f$ represents the life span that the quenching heat flux experiences.

5.3. Evaporation heat transfer

The evaporation rate is calculated as,

$$\Gamma_{vl} = \frac{\pi}{6} d_{lo}^2 \rho_v f N'' a_w \quad (83)$$

5.4. Bubble detachment size

There are quite a few models to calculate the lift-off diameter & departure diameter. [Ünal \(1976\)](#) made a correlation of bubble detachment diameter which is validated with pressure from 0.1 to 17.7 Mpa, heat flux from 0.47 to 10.64 MW/m², inlet velocity from 0.08 to 9.15 m/s, inlet subcooling from 3.0 to 86 K. [Situ et al. \(2005\)](#) developed a bubble lift-off model based on force analysis. Their test runs were performed at 1 bar, and the model was validated with heat flux from 60.7 to 206 kW/m², inlet velocity from 0.487 to 0.939 m/s, inlet subcooling from 1.5 to 20 K. [Krepper and Rzehak \(2011\)](#) developed a correlation against the experimental data directly,

$$d_{lo} = d_{\text{ref}} \exp\left(-\frac{T_{\text{sat}} - T_l}{\Delta T_{\text{refd}}}\right) \quad (84)$$

where the reference value could be found at [Krepper and Rzehak \(2011\)](#) for certain experiment.

5.5. Bubble detachment frequency

A simple estimation of the bubble departure frequency as the terminal rise velocity over the departure size is used here,

[Ceumern-Lindenstjerna \(1977\)](#),

$$f = \sqrt{\frac{4(\rho_l - \rho_v)g}{3\rho_l d_{lo}}} \quad (85)$$

5.6. Active nucleation site density

A few models have been implement in the current solver ([Lemmert and Chwala, 1977](#); [Hibiki and Ishii, 2003](#); [Krepper et al., 2007](#); [Krepper and Rzehak, 2011](#)). Here the [Krepper and Rzehak \(2011\)](#) model is used for the validation.

$$N'' = N_{\text{ref}} \left(\frac{T_w - T_l}{\Delta T_{\text{refN}}}\right)^p \quad (86)$$

The reference value can be found in [Krepper and Rzehak \(2011\)](#).

5.7. Liquid bulk temperature

Another issue arises from the bulk liquid temperature. Here we used

$$T_{\text{bulk}} = T_w - \frac{T_w^+}{T_{\text{cell}}^+} (T_w - T_{\text{cell}}) \quad (87)$$

which is already implemented in ANSYS CFX5. The bulk temperature is obtained by setting $y_{\text{bulk}}^+ = 250$. Here the subscript *cell* refers to the cells adjacent to walls.

6. Test cases

Two data sets were considered in calculations: the void fraction measurements performed by Bartolomej for subcooled boiling heat transfer to water under 45 bar pressure (Kurul, 1990; Krepper et al., 2007) and subcooled boiling heat transfer to refrigerant R-12 performed in the DEBORA experiment (Yao and Morel, 2004; Krepper and Rzehak, 2011).

The experiment conditions used as test case are listed in Table 1.

Table 1: Selected test cases and their experiment conditions

Case	Working fluid	Pressure (bar)	Mass flow rate (kg/m ² /s)	q_w'' (kW/m ²)	T_{in} (°C)
Bart	water	45	900	570	199.24
DEB5	R-12	26.15	1986	73.89	68.52
DEB6	R-12	26.15	1984.9	73.89	70.53

The tests were simulated in a quasi-two-dimensional cylindrical geometry, with 100 meshes in the axial direction and 20 meshes in the radial direction. The center of the grid cell adjacent to the wall has a non-dimensional coordinate of $y^+ = 60$ in Bartolomej test and $y^+ = 100$ in DEBORA test, approximately. Grid refinement study performed by Krepper and Rzehak (2011) for the DEBORA experiment indicates that these values of y^+ provide grid-independent solutions. The boundary condition for liquid enthalpy adopted the *fixedGradient* type in order to account for the applied wall heat flux into liquid (see in Eqn. 14), as,

$$\nabla_f^\perp h_l = \frac{a_i q_{li}'' + a_w q_{lw}''}{\beta \rho_l \kappa_l^{\text{eff}}} \quad (88)$$

The mass conservation and energy conservation over the whole pipe are carefully checked in the steady state. A typical error is $\Delta G/G_{in} = 0.048\%$ and $\Delta q''/q_w'' = 1.6\%$.

In this test case, the following interfacial models are selected:

1. Drag force: Ishii and Zuber (1979)
2. Lift force: Tomiyama (1998)
3. Wall lubrication force: Tomiyama (1998)
4. Turbulent dispersion force: Lopez de Bertodano (1992)

Figure 1 shows the comparison between the experimental and calculation results for the Bartolomej experiment, using the Yao and Morel (2004) models with $C_{td} = 2.5$. Since we used a uniformly distributed temperature profile as the inlet boundary condition for the energy conservation equation, there is a discrepancy between the predicted and measured temperature in the region nearby, as shown in Fig. 1b. However, the temperature of the bulk and at the centerline could be well predicted after the flow becomes fully developed. The averaged void fraction is somehow underestimated, which may be due to several reasons. Firstly, we used a two-equation interfacial area concentration model in which the condensation rate could be overestimated due to underestimated bubble size. Unfortunately, the measurement of the bubble size is not available in the Bartolomej experiment, rendering it difficult to evaluate the prediction of the bubble size. Secondly, the underestimation of void fraction could be also related to the modeling of

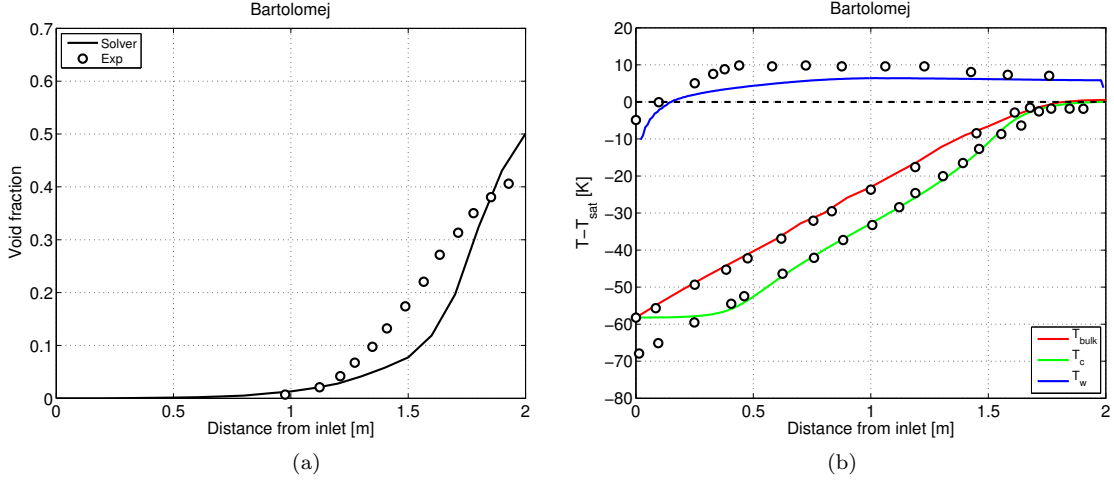


Figure 1: Axial steady state distribution of void fraction in Bartolomej experiment

interfacial forces, for example, turbulent dispersion force. If we have a large turbulent dispersion force that drives bubbles towards the cold bulk, the condensation could also be overestimated and results in a rather low void fraction. Thirdly, the observed discrepancy could also result from the underestimation of evaporation rate, which depends on the wall heat partitioning model.

Figures 2 - 4 show the comparison between the measured and predicted results of DEBORA experiment. Two sets of breakup and coalescence models were tested in our simulation. One should notice that Yao and Morel (2004) breakup and coalescence model is used together with their turbulence modeling and Lo and Zhang (2009) breakup and coalescence model together with the standard $k - \epsilon$ model. In addition, the sensitivity of turbulent dispersion force coefficient was tested here. The suggested value of C_{td} is usually in the region $[0.1, 1.0]$ for bubbly flow. However $C_{td} = 1.0$ is not sufficient enough to push the evaporation bubbles away from the surface, leading to an accumulation of void fraction near the wall, as shown in Fig. 2a. Due to that the local void fraction close to the wall may reach too high levels (above 0.74) exceeding the limits of the applicability of the present bubbly flow model. That is why we could not do the simulation with Lo and Zhang (2009) model together with $C_{td} = 1.0$ in case of DEB6, as shown in Fig. 2b.

In general, a quite satisfactory agreement between the measured and the calculated void fraction distribution has been obtained. In particular, Fig. 2b reveals that significant improvement in over-all accuracy can be obtained by choosing the turbulence dispersion force coefficient in the range between 1.0 and 2.5. The accuracy of prediction of bubble size is, however, not satisfactory. As shown in Fig. 3a, the bubble size is significantly underestimated in the observation part of the test section. This could be caused by underestimation of the bubble coalescence rate in this region. The results indicate that more work is needed to improve the interfacial area transport models. Figure 4 shows a very good agreement between predicted and measured radial temperature distributions

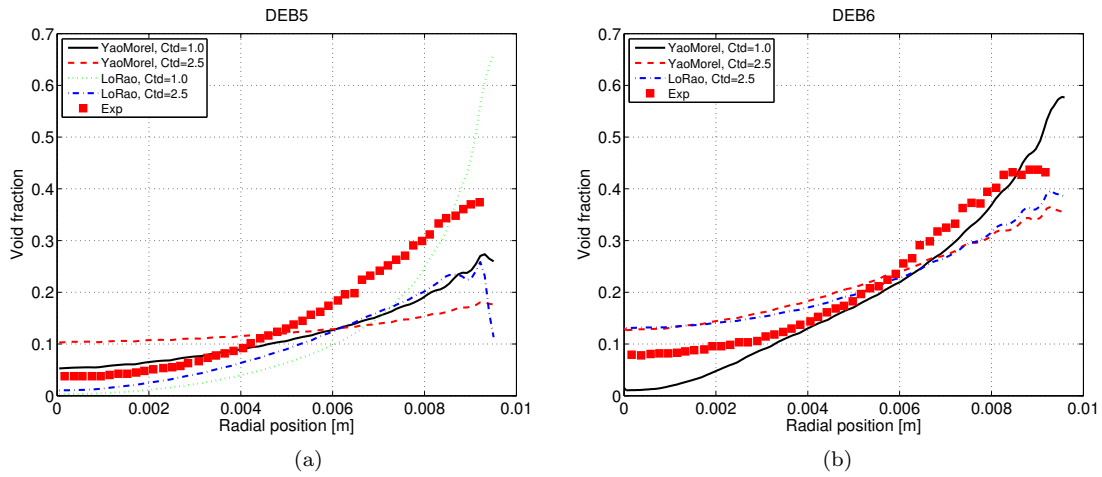


Figure 2: Comparison between the DEBORA experiment and calculation results: Radial void fraction

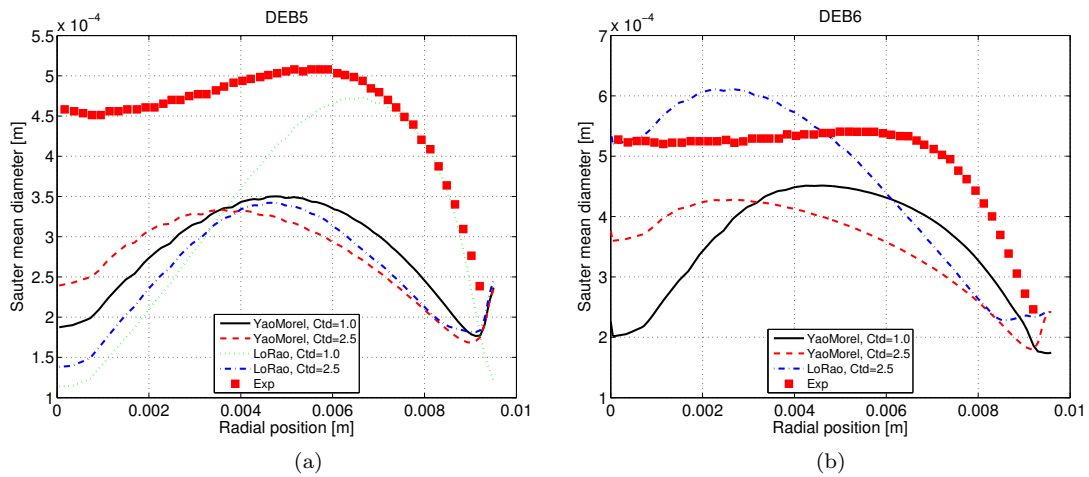


Figure 3: Comparison between the DEBORA experiment and calculation results: Radial Sauter mean diameter

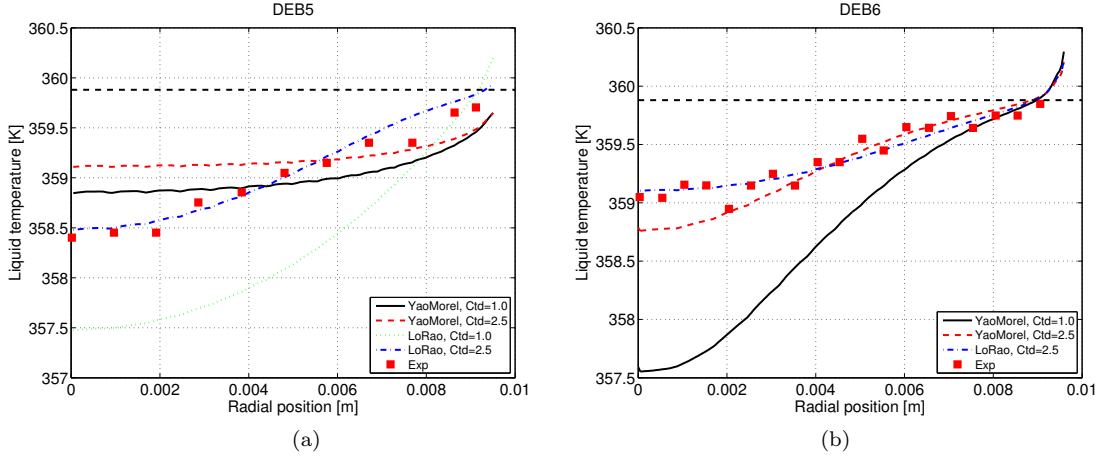


Figure 4: Comparison between the DEBORA experiment and calculation results: Radial liquid temperature

for both cases.

7. Conclusion

A two-fluid boiling flow model has been implemented into the OpenFOAM solver and validated against the Bartolomej and the DEBORA experimental data. The model includes the closure relationships for the heat transfer and phase change for bubbles moving in a subcooled liquid. Bubble size is predicted from the interfacial area concentration transport equations, including the source and sink terms resulting from the bubble coalescence and breakup, nucleation at walls as well as phase change induced source term. The present model has been validated against measurements performed in a vertical upward flow in a heated pipe. The prediction of void fraction as well as the liquid temperature profile could be done with quite satisfactory accuracy. The accuracy of prediction of the bubble size distribution is found quite low, indicating that still more work is needed to improve the interfacial area transport models.

8. Acknowledgments

Financial supports from NORTHNET, as well as support from the Swedish National Infrastructure for Computing are gratefully acknowledged.

Nomenclature

A	area fraction
a_i	interfacial area concentration, m^{-1}
C	interfacial force coefficient
c_{ti}	heat transfer coefficient given by Eqn. 67, $\text{kg}\cdot\text{m}^{-2}\cdot\text{s}^{-1}$
c_p	specific heat, $\text{J}\cdot\text{kg}^{-1}\cdot\text{K}^{-1}$
c_{vi}	heat transfer coefficient given by Eqn. 72, $\text{kg}\cdot\text{m}^{-3}\cdot\text{s}^{-1}$
D_S	Sauter mean diameter, m
d	diameter, m
d_h	hydraulic diameter, m
Eo	Eotvos number
f	bubble departure frequency, s^{-1}
G	turbulent production, $\text{kg}\cdot\text{m}^{-1}\cdot\text{s}^{-3}$ or mass flow rate, $\text{kg}\cdot\text{m}^{-2}\cdot\text{s}^{-1}$
g	gravity constant, $\text{m}\cdot\text{s}^{-2}$
h	enthalpy, $\text{J}\cdot\text{kg}^{-1}$
h_{fc}	single phase convective heat transfer coefficient, $\text{W}\cdot\text{m}^{-2}\cdot\text{K}^{-1}$
h_{fg}	latent heat, $\text{J}\cdot\text{kg}^{-1}$
h_q	quenching heat transfer coefficient, $\text{W}\cdot\text{m}^{-2}\cdot\text{K}^{-1}$
Ja	Jacob number
k	turbulent kinetic energy, $\text{m}^2\cdot\text{s}^{-2}$
\mathbf{M}	interfacial momentum transfer rate, $\text{kg}\cdot\text{m}^{-2}\cdot\text{s}^{-2}$
N''	active nucleation site density, m^{-2}
Nu	Nusselt number
\mathbf{n}_w	unit vector normal to wall
Pe	Péclet number
Pr	Prandtl number
p	pressure, Pa
q'', \mathbf{q}''	heat flux, $\text{W}\cdot\text{m}^{-2}$
q'''	heat flow rate per unit volume, $\text{W}\cdot\text{m}^{-3}$
Re	Reynolds number
T	temperature, K
t	time, s
\mathbf{U}	velocity, $\text{m}\cdot\text{s}^{-1}$
u_τ	friction velocity, $\text{m}\cdot\text{s}^{-1}$
We	Weber number

Greek letters

α	void fraction
β	void fraction for continuous phase
ϵ	turbulent dissipation rate, $\text{m}^2\cdot\text{s}^{-3}$
Γ	rate of phase change, $\text{kg}\cdot\text{m}^{-3}\cdot\text{s}^{-1}$

κ	thermal diffusivity, $\text{m}^2\cdot\text{s}^{-1}$
λ	thermal conductivity, $\text{W}\cdot\text{m}^{-1}\cdot\text{K}^{-1}$
μ	dynamic viscosity, $\text{kg}\cdot\text{m}^{-1}\cdot\text{s}^{-1}$
ν	kinematic viscosity, $\text{m}^2\cdot\text{s}^{-1}$
ψ	factor depending on bubble shape
ρ	density, $\text{kg}\cdot\text{m}^{-3}$
σ	interfacial tension, $\text{N}\cdot\text{m}^{-1}$
$\boldsymbol{\tau}$	stress tensor, $\text{N}\cdot\text{m}^{-2}$
τ_w	wall shear stress, $\text{N}\cdot\text{m}^{-2}$

Superscripts

eff	effective
d	drag
l	lift
t	turbulence
td	turbulent dispersion
vm	virtual mass
w	wall
wl	wall lubrication

Subscripts

1Φ	single phase
BB	bubble breakup
BC	bubble coalescence
b	bubble
c	convection
fc	single phase forced convection
i	interphase
k	phase
l	liquid
lo	lift-off
NUC	nucleation
q	quenching
r	relative
ref	reference
sat	saturation
v	vapor
w	wall

References

- Antal, S., Laheyjr, R., Flaherty, J., 1991. Analysis of phase distribution in fully developed laminar bubbly two-phase flow. *Int. J. Multiphase Flow* 7, 635–652.
- Bae, B., Yoon, H., Euh, D., Song, C., Park, G., 2008. Computational analysis of a subcooled boiling flow with a one-group interfacial area transport equation. *J. Nucl. Sci. Technol.* 45, 341–351.
- Lopez de Bertodano, M., 1992. Turbulent bubbly two-phase flow in a triangular duct. Ph.D. thesis. Rensselaer Polytechnic Institute. Troy, NY.

- Ceumern-Lindenstjerna, W.V., 1977. Bubble departure diameter and release frequencies during nucleate pool boiling of water and aqueous nacl solutions, in: Hahne, E., Grigull, U. (Eds.), Heat transfer in Boiling. Academic Press and Hemisphere.
- Del Valle, V.H., Kenning, D.B.R., 1985. Subcooled flow boiling at high heat flux. *Int. J. Heat Mass Transfer* 28, 1907–1920.
- Frank, T., 2005. Advances in computational fluid dynamics (cfd) of 3-dimensional gas-liquid multiphase flows, in: NAFEMS Seminar “Simulation of Complex Flows (CFD)”, Wiesbaden, Germany. p. 1.
- Gosman, A.D., Lekakou, C., Politis, S., Issa, R.I., Looney, M.K., 1992. Multidimensional modeling of turbulent two-phase flow in stirred vessels. *AIChE J.* 38, 1946–1956.
- Hibiki, T., Ishii, M., 2002. Development of one-group interfacial area transport equation in bubbly flow systems. *Int. J. Heat Mass Transfer* 45, 2351–2372.
- Hibiki, T., Ishii, M., 2003. Active nucleation site density in boiling systems. *Int. J. Heat Mass Transfer* 46, 2587–2601.
- Ishii, M., Zuber, N., 1979. Drag coefficient and relative velocity in bubbly, droplet or particulate flows. *AIChE J.* 25, 843–855.
- Kader, B.A., 1981. Temperature and concentration profiles in fully turbulent boundary layers. *Int. J. Heat Mass Transfer* 24, 1541–1544.
- Krepper, E., Koncar, B., Egorov, Y., 2007. CFD-modeling of subcooled boiling - Concept, validation and application to fuel assembly design. *Nucl. Eng. Des.* 237, 716–731.
- Krepper, E., Rzehak, R., 2011. CFD for subcooled flow boiling: Simulation of debora experiments. *Nucl. Eng. Des.* 241, 3851–3866.
- Kurul, N., 1990. Multidimensional effects in two-phase flow including phase change. Ph.D. thesis. Rensselaer Polytechnic Institute. Troy, NY.
- Kurul, N., Podowski, M.Z., 1990. Multidimensional effects in forced convection subcooled boiling, in: Proceedings of the 9th International Heat Transfer Conference, Jerusalem, Israel. p. 21.
- Kurul, N., Podowski, M.Z., 1991. On the modeling of multidimensional effects in boiling channels, in: Proceedings of the 27th National Heat Transfer Conference, Minneapolis, Minn, USA.
- Lemmert, M., Chwala, J.M., 1977. Influence of flow velocity on surface boiling heat transfer coefficient, in: Hahne, E., Grigull, U. (Eds.), Heat transfer in Boiling. Academic Press and Hemisphere.
- Lo, S., Zhang, D., 2009. Modeling of break-up and coalescence in bubbly two-phase flows. *The Journal of Computational Multiphase Flows* 1, 23–38.
- Rusche, H., 2002. Computational fluid dynamics of dispersed two-phase flows at high phase fractions. Ph.D. thesis. Imperial College. London.
- Sato, Y., Sekoguchi, K., 1975. Liquid velocity distribution in two-phase bubbly flow. *Int. J. Multiphase Flow* 2, 79–95.
- Schiller, L., Naumann, Z., 1935. A drag coefficient correlation. *Z. Ver. Deutsch. Ing.* 77, 318–320.
- Situ, R., Hibiki, T., Ishii, M., Mori, M., 2005. Bubble lift-off size in forced convective subcooled boiling flow. *Int. J. Heat Mass Transfer* 48, 5536–5548.
- Steiner, H., Kobor, A., Gebhard, L., 2005. A wall heat transfer model for subcooled boiling flow. *Int. J. Heat Mass Transfer* 48, 4161–4173.
- Tomiyama, A., 1998. Struggle with computational bubble dynamics, in: Third International Conference on Multiphase Flow.
- Ünal, H.C., 1976. Maximum bubble diameter, maximum bubble-growth time and bubble-growth rate during the subcooled nucleate flow boiling of water up to 17.7 MN/m². *Int. J. Heat Mass Transfer* 19, 643–649.
- Yao, W., Morel, C., 2004. Volumetric interfacial area prediction in upward bubbly two-phase flow. *Int. J. Heat Mass Transfer* 47, 307–328.